AIP Advances

Structural and electrical properties of lithium substituted niobo vanadate glasses doped with nickel ferrite

Cite as: AIP Advances **11**, 035210 (2021); https://doi.org/10.1063/5.0035979
Submitted: 02 November 2020 . Accepted: 07 February 2021 . Published Online: 04 March 2021

Belay G. Hailemariam, Gajanan V. Honnavar, Mohamed Irfan I, and Ramesh Keralapura

View Online Export Citation CrossMark

ARTICLES YOU MAY BE INTERESTED IN

On the correlation of the magnetic properties with the structural parameters in Fe-doped europium chromite
AIP Advances **11**, 035205 (2021); https://doi.org/10.1063/9.0000010

Influence of a split double concentric ring resonator elements axial rotation on the microwave transmission line frequency-selective characteristics
AIP Advances **11**, 035209 (2021); https://doi.org/10.1063/5.0039667

Micro-optics for ultra-intense lasers
AIP Advances **11**, 035214 (2021); https://doi.org/10.1063/5.0038023

AIP Publishing

© 2020 Author(s).

Structural and electrical properties of lithium substituted niobo vanadate glasses doped with nickel ferrite

Cite as: AIP Advances 11, 035210 (2021); doi: 10.1063/5.0035979
Submitted: 2 November 2020 • Accepted: 7 February 2021 •
Published Online: 4 March 2021

View Online Export Citation CrossMark

Belay G. Hailemariam,[1] Gajanan V. Honnavar,[1,a),b)] Mohamed Irfan I,[2] and Ramesh Keralapura[3]

AFFILIATIONS

[1]Department of Physics, College of Science, Bahir Dar University, Amhara Region, Bahirdar-79, Ethiopia
[2]Department of Mechanical Engineering, PES University South Campus, Hosur Road, Near Electronic City, Karnataka, Bangalore 560 100, India
[3]Department of Physics, Indian Institute of Science, Karnataka, Bangalore 560012, India

[a)]**Author to whom correspondence should be addressed:** gajanan.honnavar@gmail.com.
Mobile: (91) 9845166113; (+251) 904905004
[b)]**On sabbatical leave from:** PES University, South Campus, Hosur Road, Near Electronic City, Karnataka, Bangalore 560100, India.

ABSTRACT

This article reports on the impedance spectroscopic study of lithium substituted niobo vanadate glasses and their nickel ferrite doped counterparts using Cole–Cole (Nyquist) plots and electrical conductivity analysis. The glass samples were prepared using the melt quenching technique. Differential scanning calorimetry and x-ray diffractometry were used to determine the thermal properties and the amorphous nature of the glass samples, respectively. Using impedance spectroscopy, the nature and extent of inhomogeneity were investigated and correlated with transport properties in the glasses at different temperature ranges (120–240 °C). Equivalent circuit analysis was adopted to study the glass materials further. The introduction of a constant phase element (Q) in a modified RQ circuit describes the Cole–Cole plot well, which accounts for the frequency dependence of dielectric response. The electrical conductivity analysis is performed using Jonscher's law and Arrhenius plots. The exponent "*n*" was found to be a decreasing function of temperature. The DC part of the electrical conductivity is analyzed on the basis of alkali ion distance and alkali-oxygen distance. The activation energy estimated by the Arrhenius equation is found to decrease from 0.54 to 0.39 eV as lithium content increases. The estimated mobility of lithium ions was found to decrease as the lithium content increases in both doped and undoped cases.

© 2021 Author(s). All article content, except where otherwise noted, is licensed under a Creative Commons Attribution (CC BY) license (http://creativecommons.org/licenses/by/4.0/). https://doi.org/10.1063/5.0035979

I. INTRODUCTION

The demand for energy is ever increasing because of rapidly increasing worldwide population and urbanization. Developing different methods to produce energy sustainably is the need of the hour. Rechargeable batteries are one such method. Semiconducting transition metal oxides (TMOs) are candidates for this kind of energy source. Among TMO materials, vanadate glasses containing lithium ions are considered to be a potential entrant.[1,2] Lithium ion conducting solid electrolyte materials attract great attention from both scientific and technological perspectives because of their light weight, compact size, and highly electropositive characteristics, which are considered factors that contribute high energy densities and high voltages.[3,4] Vanadium based oxides are interesting among TMOs as they exhibit various oxidation states. On the basis of experimental techniques like solid state nuclear magnetic resonance (NMR) and electron paramagnetic resonance (EPR), it is established that vanadium exhibits both four- and five-fold coordination in glasses.[5,6] Both polaronic and ionic conductivity are observed in vanadate glasses. It has been reported that the incorporation of V_2O_5 improved the lithium ion conductivity in Li_2O–B_2O_3 glass.[7] V_2O_5 is a conditional glass former. It needs a co-glass

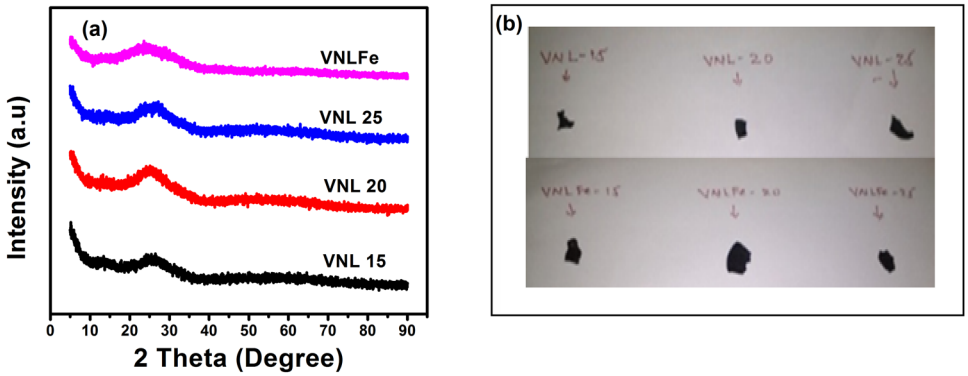

FIG. 1. (a) XRD of niobo vanadate glasses. At the top, XRD of nickel ferrite doped niobo vanadate glass is shown for comparison. The doped glass shows the same homogeneity and amorphous nature as the parent glass. (b) The photograph of the prepared glasses. The glasses were dark brown in color and were opaque.

former like another transition metal oxide to form glass. Alkali or alkali earth oxides are usually used as glass modifiers.

We preferred synthesizing ternary vanadate glasses with niobium oxide acting as a co-former since they widely differ in their valance state and atomic radius. Niobium has higher ionic radii (215 pm) than vanadium (205 pm). Hence, the effect of substituting niobium with lithium on conductivity is interesting. Furthermore, it is essential that ion conducting glasses should be chemically stable for any practical use. In a recent article, we have shown that doping nickel ferrite (NF) enhances the thermal stability of lithium substituted niobo vanadate glasses.[8]

Impedance Spectroscopy (IS) is a better method for investigation of ion movement in the frequency range of a few Hz to a few MHz in glasses.[9] A better insight into conductivity and the transport mechanism can be obtained by varying the temperature because it has a link with the change in network structure and mobility of the modifying ions. The data from IS can be modeled in terms of equivalent circuits that can give insight into the transport mechanisms of materials and device operation. For a dielectric with a single relaxation mechanism with a corresponding single relaxation time, the Cole–Cole plot is expected to be a semicircle.

This work presents a detailed analysis of temperature and frequency dependence on conductivity and Cole–Cole analysis of lithium substituted niobo vanadate (VNL) glasses and their nickel ferrite (NF) doped counterparts (VNLFe). Cole–Cole plots and equivalent circuits were used to estimate the contribution from various relaxing elements. Jonscher's equation was used to extract the values of exponent "*n*." Arrhenius plots are used to calculate the activation energy for DC conductivity. Conductivity variation vs ion separation is plotted to check how the distances between ions affect the conductivity.

II. EXPERIMENTAL DETAILS

Glasses having a general formula 70 V_2O_5–(30-x) Nb_2O_5–x Li_2O and 68 V_2O_5–(30-x) Nb_2O_5–x Li_2O–2$NiFe_2O_4$ were prepared by the melt quenching technique.[10] Nickel Ferrite ($NiFe_2O_4$) (NF) was prepared via the combustion technique (a mixture of nickel nitrate and ferric nitrate in ethyl alcohol was used as the dopant[11]). 2 mol. % of NF was doped at the expense of V_2O_5. The glasses were opaque and were dark brown in color [Fig. 1(b)]. Table I details out the glass content for ready reference.

Electrical properties were analyzed in terms of the Cole–Cole plot (Nyquist plot) and electrical conductivity formalism. Impedance measurements were recorded for temperatures ranging from 120 °C to close to T_g of the glass samples. Frequency dependent complex conductivity $\hat{\sigma} = {}^{k}/_{\hat{Z}}$, where $\hat{Z}$ is the frequency dependent complex impedance measured from the impedance analyzer and k, the cell constant given by d/A (where d is the thickness and A is

TABLE I. Glass content in mol. %, glass transition temperature (T_g) in °C, density in g/cc, and molar volume calculated using density.

Sample no.	Sample code	Glass content (mol. %) V_2O_5	Nb_2O_5	Li_2O	$NiFe_2O_4$	T_g (°C) ± 0.05 °C	Density (g/cc) ± 0.001 g/cc	Molar volume V_m (cc)
1	VNL 15	70	15	15	0	236	2.863	5996.78
2	VNL 20	70	10	20	0	252	2.932	5453.64
3	VNL 25	70	5	25	0	238	2.888	5127.14
4	VNLFe 15	68	15	15	2	261	3.108	5557.44
5	VNLFe 20	68	10	20	2	265	3.04	5321.54
6	VNLFe 25	68	5	25	2	249	2.962	5034.67

© Author(s) 2021

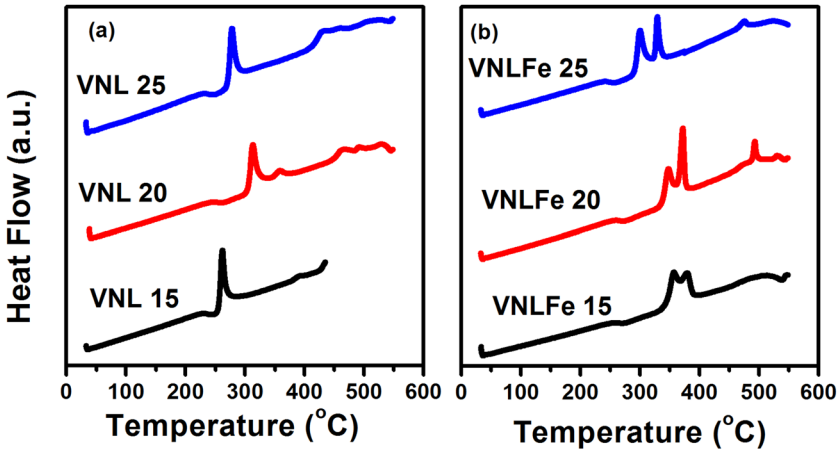

FIG. 2. Differential Scanning Calorimetry (DSC) isotherms of glasses: (a) isotherms for undoped niobo vanadate glasses and (b) isotherms for NF doped glasses.

the area of cross section of the sample), was calculated for each sample at different temperatures.[10,12]

III. RESULTS AND DISCUSSION

A. Basic characterization of glass and nickel ferrite

The amorphous nature of the glasses was confirmed by XRD [Fig. 1(a)]. Differential scanning calorimetry (DSC) was used to find the glass transition temperature (T_g). Archimedes' technique was used (with xylene as the immersion liquid) to determine the density of the prepared glass samples (details are provided in the supplementary material). The values of T_g and density are listed in Table I, and DSC isotherms of the samples are shown in Fig. 2. The prepared NF was subjected to XRD and FTIR (see Figs. S1 and S2 in the supplementary material). When doped, NF mixes homogeneously in glass and does not separate out as a different phase. This can be confirmed from perusal of Fig. 1 where along with the undoped glasses, XRD of NF doped glass is also shown for comparison. Figure 3 shows the high resolution SEM image of the prepared NF. A closer look reveals that the sample is uniform, with almost spherical structural morphology and narrow size distribution but with agglomeration to some extent. Other low resolution SEM images are presented in the supplementary material.

Since the doped glasses did not show any inhomogeneity in XRD, it felt unnecessary to record SEM or TEM images of those glasses. The presence of NF in glass was confirmed by the presence of the Fe–O bond using FTIR. Figure 4 shows clearly that the Fe–O bond present in NF is retained in the doped glass as well, whereas in the undoped counterpart, the vibrational band is absent.

Nickel ferrite present in the doped samples acts to enhance the thermal stability of the doped glasses. As can be seen from Fig. 2, the difference between T_g and the onset of crystallization is larger in doped glasses than their undoped counterparts. This is a measure of thermal stability. The increase in thermal stability in doped

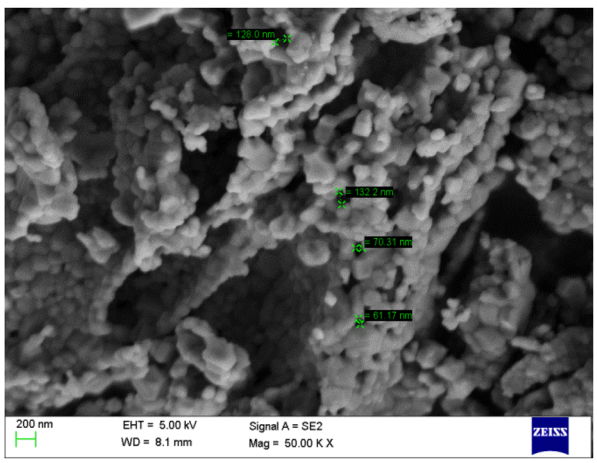

FIG. 3. High resolution SEM image of nickel ferrite.

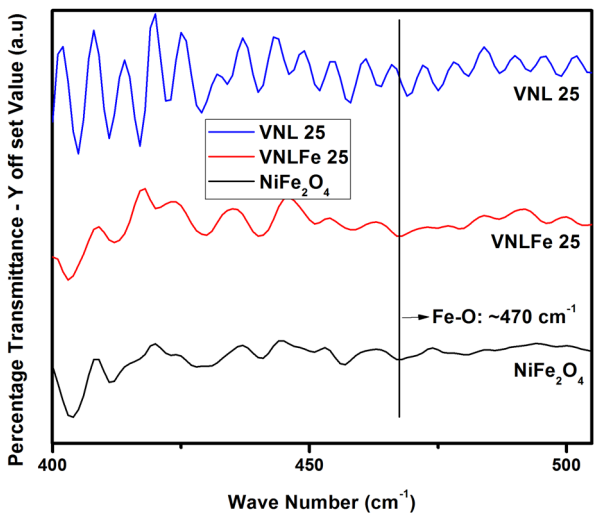

FIG. 4. Fe–O band in FTIR of NF and glass samples. The presence of this bond in NF doped representative glass (VNLFe 25) is a confirmation of doping.

© Author(s) 2021

glasses may be due to the increased packing density as the addition of nickel ferrite settles in the voids of the glass network.[8] In Ref. 8, it was shown that the addition of nickel ferrite does not impart any significant change in the DC electrical conductivity as the mol. % of added nickel ferrite is small compared with the mol. % of lithium oxide, which dictates the conductivity.

B. Cole–Cole (Nyquist) analysis

For the analysis of the impedance data using Cole–Cole (Nyquist) plots, we follow the procedure used in Ref. 13. The data were fitted with two simple parallel RC circuits with a resistor (R_p) and a capacitor (C_p). The first R_p and C_p are associated with the layer resistance and geometric capacitance of the layer of glass, respectively, while the second R_p and C_p are associated with the layer resistance and geometric capacitance of the glass/electrode interface. A contact resistance R_s (series resistance) is usually present in all glasses since there is a mismatch between the Fermi levels of the glass/electrode interface and the layer of glass near the electrode.[13] The parameters mentioned above are obtained after convergence of the fitting procedure. In the presence of series resistance (R_s) with R_p and C_p, the impedance of the circuit can be written as[13]

$$Z = R_s + \frac{R_p}{1 + i\omega R_p C_p}, \tag{1}$$

$$Z = R_s + \frac{R_p}{1 + \omega R_p C_p} - i\frac{\omega R_p^2 C_p}{1 + \omega^2 R_p^2 C_p^2} = \mathrm{Re}(Z) + \mathrm{Im}(Z). \tag{2}$$

We observe either two semicircles or one semicircle and an arc of a circle for all the glass systems under study. The semicircle at higher frequency is due to the impedance of the glass layer, and the semicircle or arc at lower frequency is related to impedance of the glass/electrode interface. These occur due to the different electrical properties and mismatch in the energy level (Fermi energy level) between these regions. For fitting, we used two parallel RC circuits connected in series. R_1 and C_1 in the circuit describe the resistance and capacitance of the bulk glass material, while R_2 and C_2 represent the resistance and capacitance of the depletion layer at the glass/electrode interface, respectively. Cole–Cole plots and the equivalent circuit fit of RC and RQ (described later in the text) for different temperatures are shown in Fig. 5 for undoped VNL glasses and in Fig. 6 for NF doped VNL glasses. The parameters extracted from the fit are listed in various tables in the supplementary material.

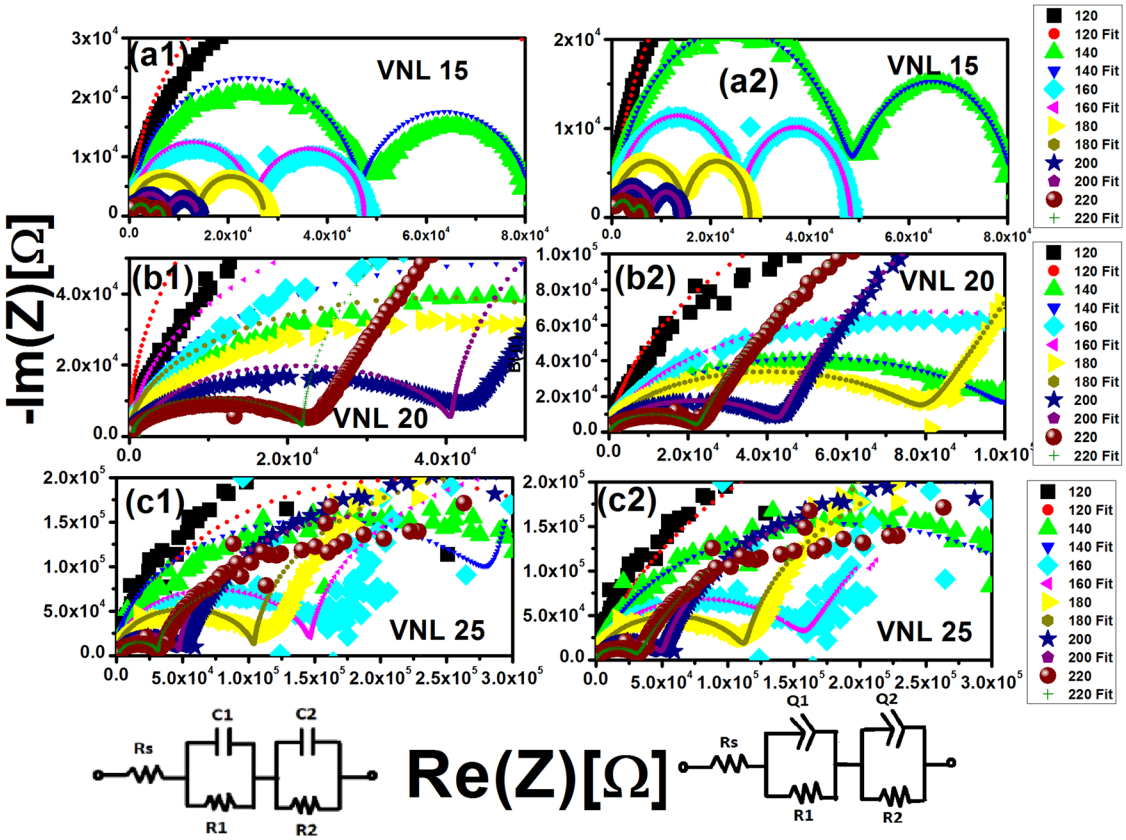

FIG. 5. Cole–Cole plots for undoped VNL glasses: (a1)–(c1) optimized fitting to the measured values at different temperatures for all glasses using equivalent circuits consisting of two RC elements and (a2)–(c2) optimized fitting using equivalent circuits consisting of two RQ elements.

© Author(s) 2021

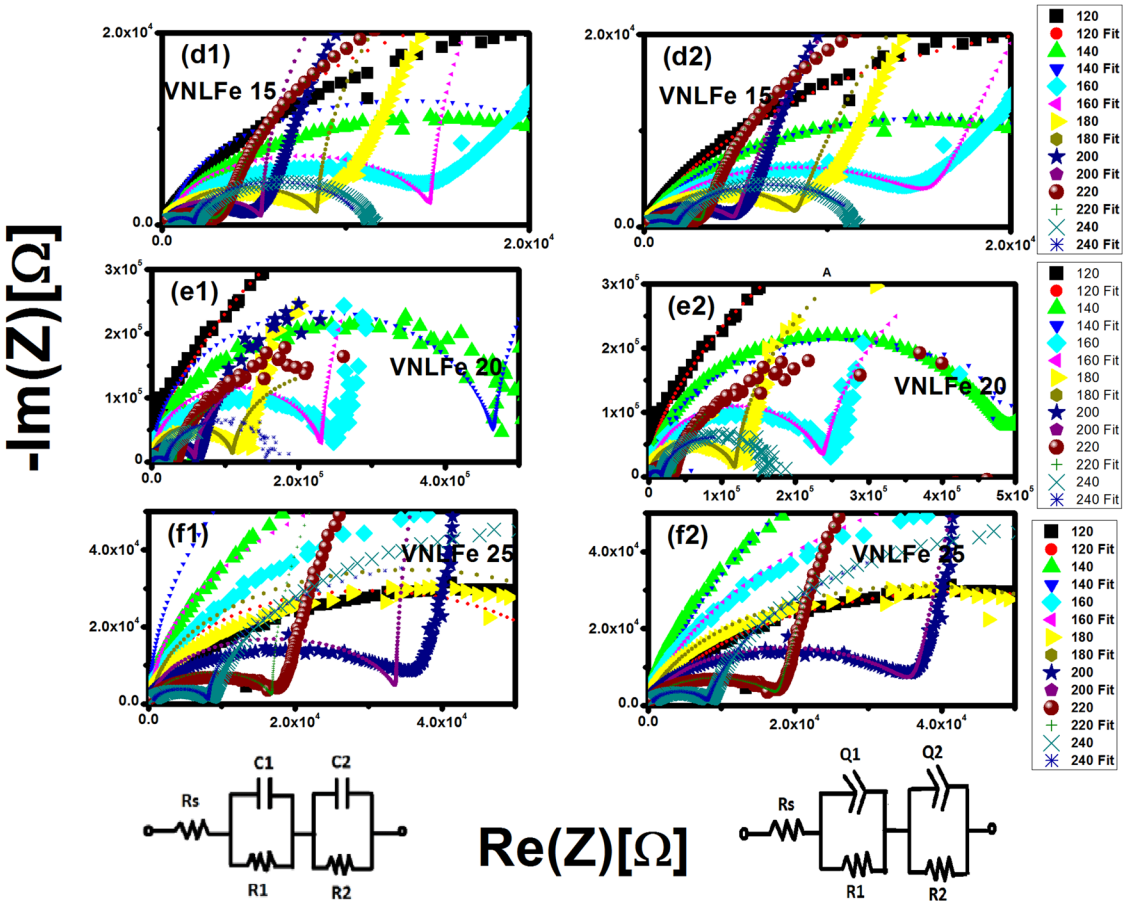

FIG. 6. Cole–Cole plots for NF doped VNL glasses: (d1)–(f1) optimized fitting to the measured Cole–Cole plots at different temperatures using equivalent circuit consisting of two RC elements and (d2)–(f2) optimized fitting using an equivalent circuit consisting of two RQ elements.

As can be seen from Figs. 5(a1)–5(c1) for undoped VNL glasses and from Figs. 6(d1)–6(f1) for NF doped VNL glasses, the two parallel RC circuits are inadequate to fit the measured data properly. This may be because a parallel RC circuit simulates an ideal Debye type of relaxation. However, in this case, the relaxation is non-Debye type due to spatial inhomogeneity or local processes like diffusion. These processes will produce a skewed or suppressed Cole–Cole plot.[9,13]

A well-established way to account for the non-Debye behavior is to replace C with a phenomenological Constant Phase Element (CPE).[9,13,14] The CPE takes account of the dispersive properties such as frequency dependent dielectric properties and provides a better fitting for the impedance characteristics of disordered materials.[14] The impedance of the CPE is written as $Z_Q = (i\omega)^{-\frac{\phi}{Q}}$, where Q is a constant and exponent ϕ is the degree of capacitive nature of the component, with values $0 < \phi < 1$. The total impedance of the RQ circuit without a series resistance can be written as[13,14]

$$Z = \frac{R_p}{1 + (i\omega)^{\phi} Q_p R_p}. \tag{3}$$

A proper fitting to the measured data was obtained with introduction of CPEs Q_1 and Q_2 in parallel with resistors R_1 and R_2. Figures 5(a2)–5(c2) and 6(d2)–6(f2) show the fitting. Thus, the non-ideal CPEs were able to correctly model the inhomogeneities and other elements responsible for the non-Debye type of relaxation. As it was mentioned earlier, the combination of R_1 and Q_1 represents the bulk glass behavior whereas the combination R_2 and Q_2 represents the glass/electrode interface. The exponent ϕ in the definition of the CPE reflects the non-ideal nature arising from various reasons in the material. Since Q_1 and hence ϕ_1 stand for bulk glass, it isϕ_1 that represents the elements responsible in relaxation. The range of variations in ϕ_1, ϕ_2, R_1, and R_2 for each glass is summarized and tabulated in Table II. The variations represent values from low temperature to high temperature. The details of the temperature range and the actual values of these parameters at those temperatures are listed in the tables given in the supplementary material.

The lower values of ϕ represent a larger inhomogeneity between relaxing sites. Hence, we may infer that different sites relax with different time scales adding up to a spread in the overall relaxation time of the glass system.

© Author(s) 2021

TABLE II. Range of some extracted parameters for each glass from RQ circuit fitting.

Glass sample	Range of ϕ_1	Range of ϕ_2	Range of R_1 (kΩ)	Range of R_2 (kΩ)
VNL 15	0.915 – 0.875	0.963 – 0.927	94.75 – 4.40	48.06 – 2.66
VNL 20	0.989 – 0.872	0.955 – 0.863	793.21 – 497.79	406.74 – 21.90
VNL 25	0.996 – 0.789	0.905 – 0.857	829.46 – 396.79	360.09 – 30.80
VNLFe 15	0.956 – 0.872	0.991 – 0.767	924.94 – 9.92	54.70 – 1.82
VNLFe 20	0.970 – 0.805	0.997 – 0.841	934.64 – 137.16	451.06 – 17.18
VNLFe 25	0.999 – 0.705	0.967 – 0.787	787.18 – 112.85	317.01 – 7.56

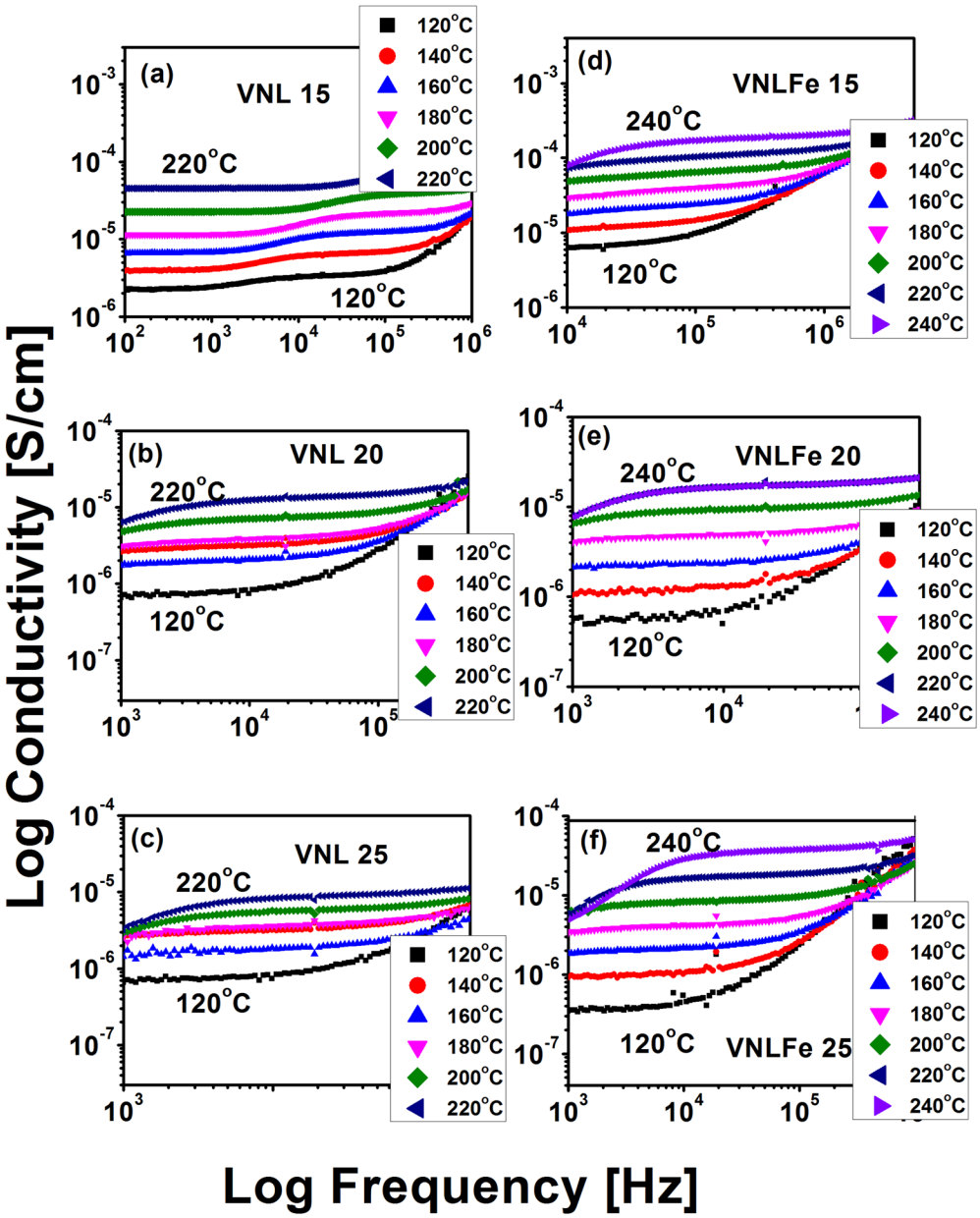

FIG. 7. Conductivity spectra of (a)–(c) undoped VNL glasses and (d)–(f) NF doped VNL glasses. The plots are for different temperatures as shown. Space charge (electrode) polarization can be observed at low frequencies. Data were noisy below the starting frequency, as shown in the figures.

© Author(s) 2021

C. Conductivity analysis

The nature of conductivity in alkali containing TMO glasses is expected to be either electronic or ionic or a mixture of both. The electron paramagnetic resonance (EPR) spectra of the present glass samples did not show hyperfine structure, confirming the absence of the V^{4+} state of the vanadium ions (see the supplementary material). Thus, we argue that the conductivity in our glass system is purely ionic.

1. Frequency dependent conductivity

Frequency dependence of conductivity can be analyzed using Jonscher's power law,[15] which, in terms of the real part of frequency dependent conductivity $\sigma'(f)$, frequency independent part (DC) conductivity σ_o , and onset frequency f_0, is written as

$$\sigma'(f) = \sigma_0\left(1 + \left(\frac{f}{f_0}\right)^n\right). \quad (4)$$

The DC conductivity σ_o can be obtained either by extrapolation of $\sigma'(f)$ to low frequencies or by extracting as a parameter from fitting Eq. (4). Figure 7 shows the conductivity spectra of all the glasses at different frequencies. Due to the polarization effect at the sample and electrode interface, the samples show a dent at low frequencies. This effect becomes significant at higher temperatures where the conductivity is high. The DC conductivity value at each temperature was taken as the conductivity $\sigma'(f_{pol})$ at a frequency f_{pol} where polarization effects set in. DC conductivities realized here are slightly higher than values reported earlier.[16] This is probably due to the different thermal history of the samples and the amount of mol. % of V_2O_5 with the lithium ion.

The spectra were fitted to Eq. (4), and the exponent "n" was extracted from the fit and is tabulated in Table III along with temperature and activation energy obtained from the Arrhenius plots [Eq. (6) and Fig. 8].

From Table III, it is observed that n is a decreasing function of temperature. It was suggested that this exponent depends on the dimensionality of the local cation conduction space such that n decreases with decreasing dimensionality.[17]

2. Frequency independent conductivity

Ionic conduction depends on the concentration and mobility of alkali ions. The ionic conductivity, σ_0, of all alkali conducting glasses is expressed as

$$\sigma_0 = Zne\mu, \quad (5)$$

where Z, n, e, and μ are the valence number of the charge carrier, concentration of charge carriers, charge, and mobility of the charge carriers, respectively. The concentration of charge carriers (i.e., concentration of Li+) is calculated from the knowledge of molar volume. From Eq. (5), the mobility of the lithium ions at 120 °C was calculated and is listed in Table IV.

In the present glass system, as the concentration of lithium ions increases, the mobility gets lower, as shown in Table IV. Murawski and Barczyński,[18] on the basis of their studies on electronic conductivity in Na_2O–FeO–P_2O_5 glasses,[19] argue that the alkali ion (Na^+ in their case) is bound to the Fe–O–P network and has lesser mobility. We consider a similar situation in our glass system and consider the possibility that Li^+ might be bounded to the V–O–Nb network. This makes Li^+ harder to separate, and the mobility decreases.

The product of σ_o (DC conductivity) and temperature T follows Arrhenius behavior below glass transition temperature. Equation (6) represents the Arrhenius equation and is used to determine the activation energy, which is tabulated in Table III,

$$\sigma_0 T = A_0 \exp\left(-\frac{E_0}{kT}\right), \quad (6)$$

where E_0 is the activation energy, k is the Boltzmann constant, and T is the temperature.

TABLE III. Temperature variation of exponent "n" and the electrical activation energy.

Sample code	Temperature (°C)	n	Activation energy (eV)
VNL 15	120	1.12	0.538
	140	1.06	
	160	1.01	
	180	0.97	
	200	0.70	
	220	0.45	
VNL 20	120	1.08	0.442
	140	0.82	
	160	0.96	
	180	0.85	
	200	0.71	
	220	0.62	
VNL 25	120	1.33	0.385
	140	1.08	
	160	1.11	
	180	0.85	
	200	0.81	
	220	0.69	
VNLFe 15	120	0.54	0.490
	140	0.44	
	160	0.47	
	180	0.43	
	200	0.30	
	220	0.20	
VNLFe 20	120	0.97	0.620
	140	1.05	
	160	0.94	
	180	0.85	
	200	0.85	
	220	0.74	
VNLFe 25	120	1.17	0.616
	140	1.10	
	160	1.04	
	180	1.00	
	200	0.67	
	220	0.52	

© Author(s) 2021

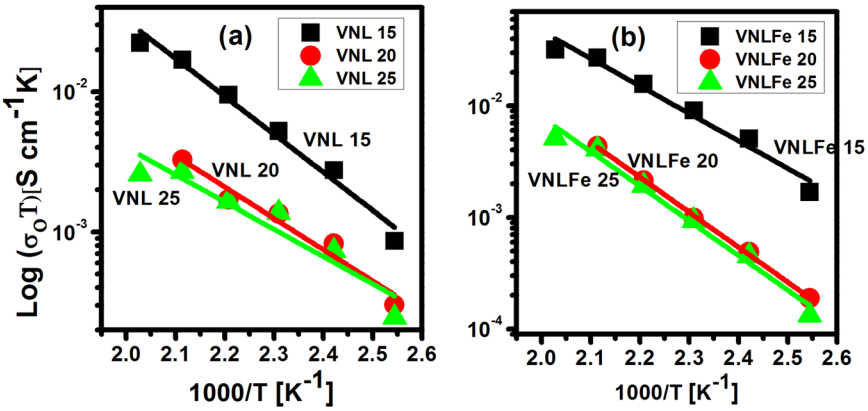

FIG. 8. Arrhenius plots for (a) undoped and (b) NF doped VNL glasses.

TABLE IV. Values of mobility of lithium ions in the present glasses.

Sample code	V_m (cc)	n(Li) (cc × 10^{19})	σ (at 120 °C) (S/cm)	μ $\left(\text{cm}^2\ \text{s}^{-1}\ \text{V}^{-1}\right) \times 10^{-7}$
VNL 15	5996.78	3.02	2.2×10^{-6}	4.55
VNL 20	5453.64	4.42	7.67×10^{-7}	1.08
VNL 25	5127.14	5.87	6.28×10^{-7}	0.67
VNLFe 15	5557.44	3.25	4.27×10^{-6}	8.20
VNLFe 20	5321.54	4.53	4.79×10^{-7}	0.66
VNLFe 25	5034.67	5.98	3.37×10^{-7}	0.35

Figure 8 presents fitting to Eq. (6) for undoped [Fig. 8(a)] and NF doped [Fig. 8(b)] VNL glasses.

As can be seen from Table III, the activation energy for undoped VNL glasses decreases from 0.538 eV to 0.385 eV with an increase in lithium concentration, whereas in NF doped counterparts, the activation energy increases from 0.49 eV to 0.62 eV. This shows that structural changes in the glass have an effect on activation energy. According to the Anderson–Stuart model,[20] the total activation energy for ionic conduction E_a is the sum of two energies given as

$$E_a = \Delta E_B + \Delta E_S, \tag{7}$$

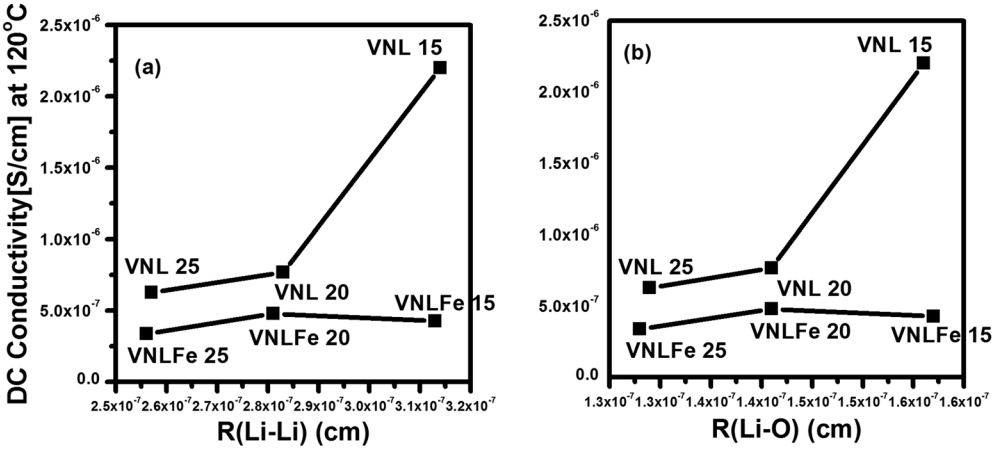

FIG. 9. DC conductivity at 120 °C vs (a) R (Li–Li) and (b) R (Li–O).

© Author(s) 2021

where ΔE_B is the electrostatic binding energy and ΔE_S is the strain energy.

A qualitative explanation is as follows: As mol. % of lithium ions increases, the covalent nature of the V–O–Li bonds changes, and that may affect the binding energy. On the other hand, the strain energy is proportional to the separation between cations. The increase in Li^+ concentration would effectively reduce the cationic distance and would reduce the strain energy. Thus, the total activation energy decreases as the concentration of lithium ions increases in the case of undoped glasses. For NF doped glasses, the activation energy increases from 0.49 eV to 0.62 eV from 15 mol. % lithium glass to 20 mol. % lithium glass and then remains at 0.62 eV for 25 mol. % glass. This sudden increase may be due to the structure becoming more rigid with NF and 20 mol. % of lithium glass than with the 15 mol. % lithium glass.

The DC conductivity at 120 °C vs R (Li–O) and R (Li–Li) is plotted in Fig. 9. The separation between cation and cation–anion was calculated from the density and molar volume.

A perusal of Fig. 9 shows that the conductivity decreases as the cationic separation or the cation–anion separation decreases. We see an appreciable change in conductivity from VNL15 to VNL20 as the separation decreases. However, in the NF doped counterpart, there is not much change in the conductivity. Ionic conductivity depends on alkali concentration and ion mobility, and one may expect electrical conductivity to increase with increasing alkali content. However, in the present glass systems, an adverse effect of increase in lithium concentration on conductivity is observed as it was mentioned earlier that lithium ions in niobo vanadate glasses have less mobility and may be bounded to the V–O–Nb network. Thus, a reduced mobility might be the cause of reduced conductivity.

IV. CONCLUSION

This work investigated the electrical conductivity of lithium substituted niobo vanadate glasses doped with nickel ferrite. Electrical conductivity for all the samples was estimated from impedance measurements. The real and imaginary parts of impedance were represented by Cole–Cole plots. Two different relaxation mechanisms at the glass/electrode interface and in bulk glass materials can be clearly seen from the nature of the Cole–Cole plots. These plots were analyzed using the equivalent circuit method consisting of an ideal resistor and a non-ideal CPE connected in parallel. The extents of inhomogeneity in the glass were determined. The electrical conductivity was analyzed using Jonscher's power law and Arrhenius plots. The power law exponent "n" was found to be a decreasing function of temperature. The variation in electrical activation energy was qualitatively explained using the Anderson–Stuart model. The conductivity is seen to decrease with cationic separation as well with cation–anion separation. This may be due to the reduced mobility of lithium ions.

SUPPLEMENTARY MATERIAL

See the supplementary material for the details of basic characterization of VNL glasses and nickel ferrite as well as tables of various parameters used to fit the Cole–Cole representation of impedance data.

ACKNOWLEDGMENTS

The authors would like to thank the central facility at the Department of Physics, IISc, Bangalore, India, for the fundamental characterization measurements. Dr. Brian Jeevan Fernandes' help in density measurements is appreciated. B.G.H. acknowledges the Management of Bahir Dar University for financial support.

DATA AVAILABILITY

The data that support the findings of this study are available from the corresponding author upon reasonable request.

REFERENCES

[1] S. Afyon, F. Krumeich, C. Mensing *et al.*, Sci. Rep. **4**, 7113 (2014).
[2] F. Zheng, M. Kotobuki, S. Song, M. O. Lai, and L. Lu, J. Power Sources **389**, 198–213 (2018).
[3] Z. Gadjourova, Y. G. Andreev, D. P. Tunstall, and P. G. Bruce, Nature **412**, 520–523 (2001).
[4] A. Manthiram, X. Yu, and S. Wang, Nat. Rev. Mater. **2**, 16103 (2017).
[5] F. R. Landsberger and P. J. Bray, J. Chem. Phys. **53**, 2757 (1970).
[6] G. V. Honnavar, K. P. Ramesh, and S. V. Bhat, J. Phys. Chem. A **118**, 573 (2014).
[7] Y. Lee, J. H. Lee, S. H. Hong, and Y. Park, Solid State Ionics **175**, 687–690 (2004).
[8] B. Getachew, K. P. Ramesh, and G. V. Honnavar, Mater. Res. Express **7**, 095202 (2020).
[9] J. R. Macdonald and E. Barsoukov, *Impedance Spectroscopy: Theory, Experiment, and Applications* (Wiley, New York, 2005).
[10] G. V. Honnavar, Ph.D. thesis, Indian Institute of Science, Bangalore, India, 2016.
[11] P. Sivakumar, R. Ramesh, A. Ramanand, S. Ponnusamy, and C. Muthamizhchelvan, Mater. Res. Bull. **46**, 2208 (2011).
[12] B. Roling, J. Non-Cryst. Solids **244**, 34 (1999).
[13] V. Varade, G. V. Honnavar, P. Anjaneyulu, K. P. Ramesh, and R. Menon, J. Phys. D: Appl. Phys. **46**, 365306 (2013).
[14] R. Schmidt, W. Eerenstein, T. Winiecki, F. D. Morrison, and P. A. Midgley, Phys. Rev. B **75**, 245111 (2007).
[15] A. K. Jonscher, Nature **267**, 673 (1977).
[16] V. Prasad, L. Pavić, A. Moguš-Milanković, A. Siva Sesha Reddy, Y. Gandhi, V. Ravi Kumar, G. Naga Raju, and N. Veeraiah, J. Alloys. Compd. **773**, 654 (2019).
[17] D. L. Sidebottom, Phys. Rev. Lett. **83**, 983 (1999).
[18] L. Murawski and R. Barczyński, Solid State Ionics **176**, 2145 (2005).
[19] L. Murawski, R. J. Barczyński, and D. Samatowicz, Solid State Ionics **157**, 293 (2003).
[20] O. L. Anderson and D. A. Stuart, J. Am. Ceram. Soc. **37**, 573 (1954).

© Author(s) 2021